Recursive Kirchhoff wavefield extrapolation

Gary F. Margrave and P.F. Daley

ABSTRACT

The theory of wavefield extrapolation by phase-shift and its extension from the Fourier domain to the space-frequency domain are reviewed. The extension of the phase-shift method to strong lateral velocity variations is also reviewed. It is shown that the space-frequency formulation developed from constant-velocity phase-shift can be trivially modified to accommodate any of three phase-shift expressions: *nonstationary phase-shift*, *phase-shift plus interpolation*, and *Weyl-form* extrapolation. These space-frequency equivalents to the Fourier methods are shown to be Kirchhoff-style summation operators that are applied by spatial convolution. Formulae for the 3-D and 2-D Kirchhoff equivalents of each of the Fourier methods are given. An extended 2-D numerical investigation shows that the Kirchhoff approach produces virtually identical results to the Fourier techniques. The importance of including the near-field term is demonstrated. An examination of algorithmic costs shows that the Kirchhoff approach can be dramatically faster than the Fourier method for strongly heterogeneous media.

INTRODUCTION

The Kirchhoff migration algorithm is probably the oldest one known, dating back at least to Hagedoorn (1954), and is currently the preferred approach in many circumstances. In part, this popularity is due to the conceptual simplicity of the approach and to the ease with which it can accommodate complex acquisition geometries. The usual Kirchhoff approach, as described in Schneider (1978) or Docherty (1991), combines Green's theorem with the scalar-wave equation to develop an expression giving any sample of the migrated image as a multi-dimensional integral through the input data. The integration takes place over a traveltime surface that is computed by tracing rays from the image point to the sources and receivers. Integration weights, that correct for such things as geometrical spreading and obliquity effects, follow from careful analysis of appropriate Green's functions. Thus, Kirchhoff methods are a blend of both wave theory and ray theory. Formulated in this way, any image point is calculated directly from a weighted summation through the seismic data. Typically, the summation surface is defined by transmission raypaths as determined by Snell's law, that is, non-Snell rays and multiple bounces are not accommodated.

Of the alternatives to Kirchhoff migration, many algorithms fall into the general category of *recursive wavefield extrapolation* (c.f. Berkhout, 1981). Also called wave-equation migration, these methods *downward-continue* the seismic data through many small depth steps. Each depth step is accomplished by a wavefield extrapolation that can be formulated using Fourier methods, finite-difference techniques, or other means. Typically, wavefield extrapolators use the assumption that, locally, constant-velocity solutions of the scalar wave equation will suffice. These methods are recursive in that the wavefield input to a given depth step is the output from the previous step.

Though they are generally more costly than Kirchhoff methods, interest in recursive wavefield extrapolation is fuelled by the observation that the resulting images are often superior to those from Kirchhoff methods (Bevc, 1997, Wyatt et al, 2000, Biondi and Vallant, 2000). A likely reason for this is that the recursive methods implicitly image along all possible transmission paths while the Kirchhoff methods only use the Snell's law path. In a limited sense, the recursive methods are analogous to a Feynman path integral in quantum mechanics while the Kirchhoff approach corresponds to a classical solution (Dickens and Willen, 2000). Since wavefield extrapolators are based upon locally constant-velocity solutions to the scalar-wave equation, Snell's law is not explicitly included as it is with Kirchhoff methods. Rather, the refraction of wavefronts by Snell's law emerges implicitly through the cascading of many extrapolation steps as a dominant, but not exclusive, propagation mode.

When velocity varies strongly with lateral position across a depth-step, finite-difference methods are often employed for wavefield extrapolation. However, the finite-difference approach suffers from a variety of complex problems such as grid dispersion, grid anisotropy in 3-D, and instability. The phase-shift method (Gazdag 1978) does not have these drawbacks but cannot handle lateral velocity variations. Recently, Fourier wavefield extrapolators have been developed that can accommodate strong lateral velocity variations (Margrave and Ferguson 1999, Ferguson and Margrave, 2001). These operators are now known to be *Fourier integral operators* (Stein 1993) and can be developed via a Taylor-series approach to the variable-velocity scalar-wave equation (Margrave and Ferguson, 2000). They are higher order approximate solutions to the wave equation that produce excellent images of test datasets but require long computation times.

In this paper, we develop space-frequency approximations to the PSPI (phase shift plus interpolation) and NSPS (nonstationary phase shift) Fourier integral operators of Margrave and Ferguson (1999). We begin with a general discussion of the mathematics required to move a constant-velocity phase-shift operator to the space-frequency domain. Then, various variable-velocity phase-shift extrapolators are presented and it is argued that our formulae for the space-frequency domain also apply directly to these. Subsequently, we develop analytic forms for space-frequency extrapolators that correspond to local Kirchhoff summation operators. The 3-D form is exact while in 2-D a high frequency approximation for the Hankel function is used to derive an approximate near-field correction. After briefly examining and discarding stationary-phase results, we present 3-D and 2-D formulae for the Kirchhoff equivalent operators for *nonstationary phase-shift* (NSPS), *phase-shift plus interpolation* (PSPI) and the *Weyl-form extrapolator*. Then follows an extended series of numerical examples in which we demonstrate that the 2-D Kirchhoff operators are nearly equivalent to the Fourier operators and we also show the importance of including the near-field term. Finally, we present a cost comparison of the Kirchhoff versus the Fourier approach. When used in a recursive wavefield extrapolation, the Kirchhoff extrapolators allow a migration algorithm that combines the best features of direct Kirchhoff methods and Fourier wavefield extrapolation with very attractive computation times. Bevc (1997) proposes recursive Kirchhoff extrapolation but does not make the link to Fourier techniques as we do here.

SPACE-FREQUENCY DOMAIN FORMULATIONS FOR FOURIER EXTRAPOLATORS

Space-frequency domain, constant-velocity extrapolation

Consider the equation for the 3-D f-k phase-shift extrapolator

$$\psi(x,y,z,\omega)=\frac{1}{4\pi^2}\int_{-\infty}^{\infty}\varphi(k_x,k_y,z=0,\omega)e^{ik_z z-ik_x x-ik_y y}dk_x dk_y \tag{1}$$

where $\psi(x,y,z,\omega)$ is a single-frequency component of a scalar wavefield at position *(x,y,z)*, $\varphi(k_x,k_y,z=0,\omega)$ is the Fourier transform (over *x* and *y*) of the wavefield at position *(x,y,z=0)*, (k_x,k_y,k_z) are components of the wavenumber vector, $k_z z$ is the extrapolation phase-shift, and the integral performs a 2-D inverse Fourier transform from $(k_x,k_y)\rightarrow(x,y)$. It is assumed that $\psi(x,y,z,\omega)$ satisfies the constant-velocity Helmholtz equation and consists only of upward-travelling waves. The vertical component of the wavenumber vector, k_z, in the phase-shift can be calculated from the other components and the frequency by

$$k_z=\sqrt{\frac{\omega^2}{v^2}-k_x^2-k_y^2} \tag{2}$$

where *v* is the wave speed, and $\varphi(k_x,k_y,z=0,\omega)$ is

$$\varphi(k_x,k_y,z=0,\omega)=\int_{-\infty}^{\infty}\int_{-\infty}^{\infty}\psi(x,y,z=0,\omega)e^{ik_x x+ik_y y}dxdy \tag{3}$$

.

Insertion of equation (3) into equation (1) and interchanging the order of integration results in

$$\psi(x,y,z,\omega)=\frac{1}{4\pi^2}\int_{-\infty}^{\infty}\psi(\hat{x},\hat{y},z=0,\omega)\left[\int_{-\infty}^{\infty}e^{ik_z z-ik_x(x-\hat{x})-ik_y(y-\hat{y})}dk_x dk_y\right]d\hat{x}d\hat{y} \tag{4}$$

where $(\hat{x},\hat{y})$ has been used to denote the input lateral coordinates of equation (3). The integral in square brackets in equation (4) is the desired space-frequency domain extrapolator. If we define

$$W_{3D}(x,y,z,v,\omega)=\frac{1}{4\pi^2}\int_{-\infty}^{\infty}e^{ik_z z-ik_x x-ik_y y}dk_x dk_y \tag{5}$$

then equation (4) can be written

$$\psi(x,y,z,\omega)=\int_{-\infty}^{\infty}\psi(\hat{x},\hat{y},z=0,\omega)W_{3D}(x-\hat{x},y-\hat{y},z,v,\omega)d\hat{x}d\hat{y}. \tag{6}$$

We call W_{3D} the three-dimensional, space-frequency, wavefield-extrapolation operator and equation (6) shows that it is applied to the wavefield by a 2-D convolution over the lateral spatial coordinates.

These arguments can be repeated for the 2-D case with the result that 2-D wavefield extrapolation is given by

$$\psi(x,z,\omega)=\int_{-\infty}^{\infty}\psi(\hat{x},z=0,\omega)W_{2D}(x-\hat{x},z,v,\omega)d\hat{x} \tag{7}$$

with W_{2D} given by

$$W_{2D}(x,z,v,\omega)=\frac{1}{2\pi}\int_{-\infty}^{\infty}e^{ik_z z-ik_x x}dk_x. \tag{8}$$

Rather than giving a separate equation for the 2D k_z, we note that it is obtained from equation (2) by simply setting $k_y=0$. We do not use separate symbols for the 2-D and 3-D k_z because it is always clear from the context which one is needed. Like 3-D wavefield extrapolator, W_{2D} is applied by spatial convolution, although in 1-D since there is only one lateral coordinate.

Advanced phase-shift extrapolators

The expressions for W_{3D} (equation 5) and W_{2D} (equation 8) were developed from the constant-velocity phase-shift extrapolator but they are easily modified to accommodate the various phase-shift operators that approximately accommodate lateral velocity variations. We list these here, in their 2-D forms, beginning with the PSPI operator

$$\psi_{PSPI}(x,z,\omega)=\frac{1}{2\pi}\int_{-\infty}^{\infty}\varphi(k_x,z=0,\omega)e^{ik_z(x)z-ik_x x}dk_x \tag{9}$$

where

$$k_z(x)=\sqrt{\frac{\omega^2}{v^2(x)}-k_x^2}. \tag{10}$$

Next, the NSPS operator

$$\varphi_{NSPS}\left(k_x,z,\omega\right)=\frac{1}{2\pi}\int_{-\infty}^{\infty}\psi\left(\hat{x},z=0,\omega\right)e^{ik_z\left(\hat{x}\right)z+ik_x\hat{x}}d\hat{x} \tag{11}$$

where $\psi_{NSPS}\left(x,z,\omega\right)$ is then recovered by an inverse Fourier transform over k_x and $k_z\left(\hat{x}\right)$ is again given by equation (10). These two forms have been extensively studied in previous CREWES Reports and elsewhere (Margrave and Ferguson, 1999, Ferguson and Margrave, 2001) and their major distinction is that equation (9) assigns the lateral velocity variation to the output coordinate while equation (11) assigns it to the input coordinate. It is also known that equation (9) is a standard-form pseudodifferential operator of the Kohn-Nirenberg form while equation (11) is an *adjoint-form* Kohn-Nirenberg pseudodifferential operator (see Stein, 1993, for definitions). A third interesting form is a pseudodifferential operator of the Weyl form (Weyl, 1931 IV.14, Wong, 1998) that has the advantage of splitting the velocity dependence between the input and output locations. The Weyl-form phase-shift extrapolator is given by

$$\psi_{Weyl}\left(x,z,\omega\right)=\frac{1}{2\pi}\int_{-\infty}^{\infty}\psi\left(x,z=0,\omega\right)e^{ik_z\left(.5x+.5\hat{x}\right)z+ik_x\left[\hat{x}-x\right]}d\hat{x}dk_x \tag{12}$$

where $k_z\left(.5x+.5\hat{x}\right)$ is still given by equation (10).

All of these advanced phase-shift operators, equations (9), (11), and (12), are derivable from the constant velocity expression, equation (1) with $k_y=0$, by simply replacing v with $v\left(x\right)$ for PSPI, replacing v with $v\left(\hat{x}\right)$ for NSPS (after moving the phase-shift operator into the implied forward Fourier integral), and replacing v with $v\left(.5x+.5\hat{x}\right)$ for the Weyl operator. This is significant in the present context because the forms for W_{3D}, equation (5), and W_{2D}, equation (8), are integrals over wavenumbers not spatial coordinates. Thus, once forms are given for the constant-velocity extrapolators in space-frequency, the various laterally variable forms follow immediately by the simple velocity replacement rule just specified. Thus it is a simple matter to make the transition from constant-velocity space-frequency domain extrapolators to extrapolators that are appropriate for extreme heterogeneity. However, the same cannot be said for anisotropy because this effect generally requires that velocity also depend upon wavenumber.

Analytic forms

The analytic forms of equations (5) and (8) are well known and can be found in many papers and texts such as Berkhout (1985). It is also well known (e.g. Robinson and Silvia 1981, p371-373) that they are expressible via the z derivatives of the corresponding 3-D and 2-D Greens functions. That is, W_{3D} is known to be given by

$$W_{3D}(x,y,z,v,\omega) = -2\frac{\partial}{\partial z} g_{3D}(x,y,z,v,\omega) \tag{13}$$

where the 3-D Greens function is

$$g_{3D}(x,y,z,v,\omega) = \frac{e^{ikr}}{4\pi r} \tag{14}$$

with $r = \sqrt{x^2+y^2+z^2}$ and $k = \omega / v$. Straightforward calculation then shows that

$$W_{3D}(x,y,z,v,\omega) = -\frac{ik\cos\theta}{2\pi r} e^{ikr}\left(1+\frac{i}{kr}\right) \tag{15}$$

where $\cos\theta = z/r = \partial r/\partial z$ is the cosine of the *scattering angle*. Equation (15) shows that W_{3D} consists of two terms, one that goes as r^{-1} and is called the *far-field term* and another that goes as r^{-2} and is called the *near-field term*.

When equation (15) is substituted into equation (6) the result can be written

$$\psi(x,y,z,\omega) = \frac{-i\omega}{2\pi}\int_{-\infty}^{\infty}\psi(\hat{x},\hat{y},z=0,\omega)\frac{z}{v\tilde{r}^2}e^{i\omega\tilde{r}/v}\left(1+\frac{iv}{\omega\tilde{r}}\right)d\hat{x}d\hat{y} \tag{16}$$

where $\tilde{r} = \sqrt{(x-\hat{x})^2+(y-\hat{y})^2+z^2}$ and $\cos\theta$ has been replaced by $z/\tilde{r}$. Equation (16) is the space-frequency equivalent of the 3-D phase-shift expression (equation 1). It is a simple integral, over the input lateral coordinates, where the integrand is the product of the input wavefield, $\psi(\hat{x},\hat{y},z=0,\omega)$, an angle-dependent geometric factor, $z/\tilde{r}^2$, a phase-shift operator, $\exp(i\omega\tilde{r}/v)$, and a near-field modifier, $1+iv/\omega\tilde{r}$. Strictly speaking, the denominator of the geometric factor could be pulled outside the integral because it has no coordinate dependence, but we prefer to leave it because such a dependence will shortly be introduced.

The phase-shift in equation (16) is precisely that required to give the time advance necessary to sum along a constant-velocity diffraction hyperboloid. Thus, the equation is a spatial convolution of the wavefield with an operator that achieves geometric scaling and summation along a diffraction hyperboloid. Accordingly, equation (16) is interpretable as a Kirchhoff-style wavefield-extrapolation operation in the space-frequency domain.

Similarly, W_{2D} is given by

$$W_{2D}(x,z,v,\omega) = -2\frac{\partial}{\partial z} g_{2D}(x,z,v,\omega) \tag{17}$$

where the 2-D Greens function is (Zauderer, 1989, p383)

$$g_{2D}(x,z,v,\omega)=\frac{i}{4}H_0^{(1)}(k\rho) \tag{18}$$

and $H_0^{(1)}(u)$ is the zero-order Hankel function of the first kind. $H_0^{(1)}(u)$ has the following series representation (Gradshteyn and Ryzhik, 1980)

$$H_0^{(1)}(u)\sim\sqrt{\frac{2}{\pi u}}e^{i[u-\pi/4]}\left[1+\frac{1}{8iu}+\cdots\right]. \tag{19}$$

For large *u*, only the first term is needed, while for the present purposes the first two terms will be used. Using the approximation (19) in equation (17) predicts

$$W_{2D}(x,z,v,\omega)\sim\cos\theta\sqrt{\frac{k}{2\pi\rho}}e^{i[k\rho-\pi/4]}\left[1+\frac{3i}{8k\rho}\right]. \tag{20}$$

Thus we have the interesting circumstance that W_{3D} is given by a simple analytic form that is valid everywhere while W_{2D} has an approximate form that cannot be expected to be valid at very small $k\rho$. (W_{2D} is know exactly as $\frac{-i}{2}\partial H_0^{(1)}(k\rho)/\partial z$ but its realization in terms of simple analytic functions is approximate.)

A final form for a 2-D extrapolator can be developed by substituting equation (20) into equation (7)

$$\psi(x,z,\omega)=z\sqrt{\frac{\omega}{2\pi}}\int_{-\infty}^{\infty}\psi(\hat{x},z=0,\omega)\sqrt{\frac{1}{v\tilde{\rho}^3}}e^{i[\omega\tilde{\rho}/v-\pi/4]}\left[1+\frac{3iv}{8\omega\tilde{\rho}}\right]d\hat{x} \tag{21}$$

where $\tilde{\rho}=\sqrt{(x-\hat{x})^2+z^2}$ and $\cos\theta$ has been replaced by $z/\tilde{\rho}$. As in the 3-D case, this expression can be interpreted as a Kirchhoff operation; but this time, in 2-D.

Stationary-phase considerations

It is very common to employ the method of stationary phase to develop approximate forms for W_{3D} and W_{2D}. The theory of stationary phase can be found in many texts (e.g. Murray, 1984, Bleistein and Handselman, 1986) and is a standard tool to deduce the leading order behaviour of oscillatory integrals like those of equations (5) and (8). The details of our stationary-phase calculations are straightforward and are not given here. The results are, for W_{3D}

$$W_{3D}(x,y,z,v,\omega)\sim-\frac{ik\cos\theta}{2\pi r}e^{ikr} \tag{22}$$

where, as before, $r=\sqrt{x^2+y^2+z^2}$ and $\cos\theta=z/r$. For

$$W_{2D} \sim \cos\theta \sqrt{\frac{k}{2\pi\rho}}\, e^{ik\rho - i\pi/4} \tag{23}$$

Comparing equation (22) with equation (15) and also comparing equation (23) with equation (20) shows that the stationary-phase approximations do not include the near-field terms from W_{3D} and W_{2D}. In most Kirchhoff algorithms this is not considered to be a serious omission because they are formulated as *direct estimation* methods. This means that each point in the subsurface is imaged with a single large extrapolation step directly from the recording geometry. However, in the present case, we desire a recursive Kirchhoff application using many small steps, and in the next section we show that the near-field terms can be significant.

Kirchhoff analogs to the advanced Fourier extrapolators

The constant-velocity formulae for the application of W_{3D} and W_{2D} (equations 16 and 21) can be directly modified to emulate the three different Fourier operators described previously. First, for PSPI we obtain the 3-D expression

$$\psi_{PSPI}(x,y,z,\omega) = \frac{-i\omega}{2\pi v(x,y)} \int_{-\infty}^{\infty} \psi(\hat{x},\hat{y},z=0,\omega) \frac{z}{\tilde{r}^2} e^{i\omega\tilde{r}/v(x,y)} \left(1 + \frac{iv(x,y)}{\omega\tilde{r}}\right) d\hat{x}d\hat{y} \tag{24}$$

with $\tilde{r} = \sqrt{(x-\hat{x})^2 + (y-\hat{y})^2 + z^2}$ and in 2-D

$$\psi_{PSPI}(x,z,\omega) = z\sqrt{\frac{\omega}{2\pi v(x)}} \int_{-\infty}^{\infty} \psi(\hat{x},z=0,\omega) \sqrt{\frac{1}{\tilde{\rho}^3}} e^{i[\omega\tilde{\rho}/v(x) - \pi/4]} \left[1 + \frac{3iv(x)}{8\omega\tilde{\rho}}\right] d\hat{x}. \tag{25}$$

with $\tilde{\rho} = \sqrt{(x-\hat{x})^2 + z^2}$. Next, the NSPS expressions are, for 3-D,

$$\psi_{NSPS}(x,y,z,\omega) = \frac{-i\omega}{2\pi} \int_{-\infty}^{\infty} \psi(\hat{x},\hat{y},z=0,\omega) \frac{z}{v(\hat{x},\hat{y})\tilde{r}^2} e^{i\omega\tilde{r}/v(\hat{x},\hat{y})} \left(1 + \frac{iv(\hat{x},\hat{y})}{\omega\tilde{r}}\right) d\hat{x}d\hat{y} \tag{26}$$

and for 2-D

$$\psi_{NSPS}(x,z,\omega) = z\sqrt{\frac{\omega}{2\pi}} \int_{-\infty}^{\infty} \psi(\hat{x},z=0,\omega) \sqrt{\frac{1}{v(\hat{x})\tilde{\rho}^3}} e^{i[\omega\tilde{\rho}/v(\hat{x}) - \pi/4]} \left[1 + \frac{3iv(\hat{x})}{8\omega\tilde{\rho}}\right] d\hat{x}. \tag{27}$$

Finally, for the Weyl operator, in 3-D we have

$$\psi_{Weyl}(x,y,z,\omega) = \frac{-i\omega}{2\pi} \int_{-\infty}^{\infty} \psi(\hat{x},\hat{y},z=0,\omega) \frac{z}{v(\tilde{x},\tilde{y})\tilde{r}^2} e^{i\omega\tilde{r}/v(\tilde{x},\tilde{y})} \left(1 + \frac{iv(\tilde{x},\tilde{y})}{\omega\tilde{r}}\right) d\hat{x}d\hat{y} \tag{28}$$

where $\tilde{x} = (x+\hat{x})/2$ and $\tilde{y} = (y+\tilde{y})/2$; and in 2-D

$$\psi_{Weyl}(x,z,\omega) = z\sqrt{\frac{\omega}{2\pi}}\int_{-\infty}^{\infty}\psi(\hat{x},z=0,\omega)\sqrt{\frac{1}{v(\tilde{x})\tilde{\rho}^3}}e^{i[\omega\tilde{\rho}/v(\tilde{x})-\pi/4]}\left[1+\frac{3iv(\tilde{x})}{8\omega\tilde{\rho}}\right]d\hat{x}. \quad (29)$$

A 2-D NUMERICAL IMPLEMENTATION

We have implemented equations (25), (27), and (29) in a Matlab code to test our conclusions and compare the recursive Kirchhoff approach to the recursive Fourier methods. Figure 1 shows a comparison of the Kirchhoff and Fourier NSPS methods. As shown in Margrave and Ferguson (1999), NSPS has the property that diffraction hyperbolae track smoothly across velocity discontinuities; and both algorithms show this behaviour. The velocity model has a discontinuous step at its centre where it changes from 2000m/s to 3000m/s. The input wavefield consisted of two impulses at equal times on either side of the velocity discontinuity. A single 50m upward step was taken. The two algorithms have produced almost identical responses. In Figure 2, the *f-k* transforms of the results of Figure 1 are shown to demonstrate that they are similar at almost all spectral points. The most distinctive differences are near the spectral origin and these are likely due to the approximate nature of the near-field term in the Kirchhoff implementation. As well, the Kirchhoff spectrum shows a line of high amplitudes near the negative evanescent boundary that are not seen in the Fourier result. Whether this is due to a difference in the numerical implementation of a dip filter in the two algorithms or is a more inherent feature is under investigation.

Figure 3 repeats the Kirchhoff result of Figure 1 and compares it with its own near-field term (in relative scale). Figure 4 displays the *f-k* transforms of these wavefields. The near-field term can be seen to contribute a small though significant part of the result. If a smaller depth-step were taken, the near-field term would be a more significant part of a diminished total response.

Figures 5 and 6 repeat the experiment depicted in Figures 1 and 2, except that this time the PSPI algorithm is compared in its Kirchhoff and Fourier implementations. Again the new Kirchhoff method has a behaviour very similar to the Fourier approach and both show the characteristic wavefield discontinuity at the velocity boundary. As with the previous example, the *f-k* spectra show that the Kirchhoff method is distinct in that it has more energy near the negative evanescent boundary than the Fourier result.

Figures 7 and 8 are again a repeat of the same experiment except that this time the Weyl operator has been used. The results are, in some sense, intermediate to the PSPI and NSPS results. As discussed in Margrave and Ferguson (1998), there are many such symmetric combinations of NSPS and PSPI and most have subtle advantages. Again, the *f-k* spectrum indicates that the Kirchhoff method has more energy near the evanescent boundaries than the Fourier result. This is possibly a shortcoming of the Kirchhoff method, although its precise cause is presently unclear.

In a second test, we consider the extrapolation of a test wavefield through the "fault" model of Figure 9. The input wavefield (Figure 10) was a series of eight impulses and was extrapolated 150m upward through the model of the previous figure. The extrapolation was done with 15 steps of 10 metres using the Fourier NSPS algorithm of equation (11). The resulting extrapolated wavefield is shown in Figure

11 and its *f-k* spectrum is in Figure 12. Each impulse has spread into a diffraction response characterized by the velocity structure above the impulse. The ensemble of diffraction responses forms a composite event that tilts up to the right. The *f-k* spectrum shows three dominant lines that tilt to the left. The success of a downward extrapolation of this wavefield can be judged both by how well the impulses are focused and by how well these spectral lines are shifted to the vertical.

The sequence of Figures 13-18 show a series of extrapolation tests that all used 5 steps of 30 metres to reconstruct the input wavefield (Figure 9) from the *test wavefield* of Figure 11. The use of a coarser set of downward steps than upward steps means that the downward reconstructions will be of lower accuracy. Figures 13 and 14 show the wavefield and its *f-k* spectrum that result from a downward extrapolation of the test wavefield using the Fourier PSPI algorithm (equation 9). The PSPI algorithm is an excellent inverse for NSPS and this image is a superior benchmark for comparison with Kirchhoff results. Figures 15 and 16 are the wavefield and its *f-k* spectrum that result from a downward extrapolation using the Kirchhoff PSPI algorithm of equation (25) using the approximate near-field term of $3iv/8\omega\rho$ (times the far-field term). The Kirchhoff reconstruction is very good and nearly identical to the Fourier result. Finally, Figures 17 and 18 repeat the Kirchhoff PSPI result except that the near-field term has been omitted. Though there is still good focusing, there is a clear degradation of the result including a noticeable phase distortion of the focal points. The *f-k* spectrum shows a slight loss of power at low frequencies near zero wavenumber.

Figures 19-25 are a second suite of downward extrapolations all conducted with 15 steps of 10 metres, just as was the upward extrapolation. In Figures 19 and 20 is the wavefield and its *f-k* spectrum that result from the Fourier PSPI algorithm. This is about as good a reconstruction as is possible without something like least-squares. Figures 21 and 22 show the result of the Kirchhoff PSPI algorithm without the approximate near-field term. This time, compared with Figures 17 and 18, there is a very pronounced phase and amplitude distortion in the image and a strong loss of power in the *f-k* spectrum. In Figures 23 and 24, the approximate near-field term is included and the result, although better, is still far from the excellent image of the Fourier PSPI. The *f-k* spectrum in Figure 24 shows that the lost power around zero wavenumber at low frequencies has been restored but, in fact, too strongly. This indicates that the approximate near-field correction developed in equation (20) is not sufficient and the next term is probably needed. In Figures 25 and 26 is another Kirchhoff PSPI but with the near-field term of $3iv/8\omega\rho$ scaled by 80% (determined empirically). The result is clearly improved. These experiments support the general conclusion that the near-field term is essential in recursive wavefield extrapolation, becoming increasingly important as the step size decreases.

COMPUTATIONAL EFFORT AND OTHER ALGORITHMIC CHARACTERISTICS

Both the Kirchhoff and Fourier versions of NSPS and PSPI scale as N^2 algorithms, meaning that computation costs go up as the square of the number of traces. This can be demonstrated either by analysis or by experiment: Figures 27-29

document the latter approach. Shown in these figures are the results of timing tests in a controlled experiment where only the number of traces was varied. The Fourier version of NSPS was compared with several different dip-limitations in the Kirchhoff version. PSPI costs the same and is not shown. In Figure 27, the CPU times are plotted versus the number of traces and it is quite apparent that the Fourier algorithm requires much more time. In Figure 28, the logarithms of time and number of traces are plotted with each line having a slope of about 2, indicating an N^2 process. Finally, in Figure 29, the ratio of the Fourier time to the Kirchhoff time is shown and it can be seen that the relative increase in speed ranges from about a factor of six for the 90-degree Kirchhoff algorithm to over 100 for the 30-degree algorithm.

The improvements in computation speed, while impressive, require clarification. First, the Fourier algorithm runs at a speed that is strongly dependent on the complexity of the velocity structure and independent of any dip limitation. Conversely, the Kirchhoff approach is independent of the velocity complexity (as long as straight raypaths are used) but strongly dependent upon the dip limitation. In these comparisons, we chose to use the direct Fourier method that implements either of equations (9) or (11) as a matrix-vector multiplication. This approach is quite general and can handle any velocity complexity but is relatively slow. For simple velocity distributions, a number of improvements can be made in the Fourier methods that can dramatically improve the computation speed. For example, in constant velocity media, the phase-shift method can be used and a huge speed increase will result while the Kirchhoff methods will run at the same speed as before.

The need for the Fourier algorithm to have zero-valued traces padded onto the sides of the data, for protection against wraparound and for improvement in FFT speed, is also a factor. The Kirchhoff methods do not require this and, especially in 3-D, this can be a huge advantage. (The “number of traces” used as the axes in Figures 27-29 is the number before any padding and so is the same for both approaches.)

Generally, the Fourier methods are more sensitive to irregularities in data geometry than the Kirchhoff algorithms. Such irregularities usually only slow down the first step in an extrapolation process as a regular output geometry can generally be synthesized regardless of the input. It is a simpler matter to modify the Kirchhoff algorithms to accommodate unusual data gathers, such as common-offset sections, than for the Fourier approaches. This is a popular approach to prestack 3D migrations that can lead to very significant economies.

Though we call our approach a Kirchhoff method, we emphasize that, unlike most other Kirchhoff methods including that of Bevc (1997), our approach does not require raytracing. In this respect, it is like phase-shift methods where traveltimes are computed geometrically assuming straight raypaths. As with other recursive methods, the cascade of many steps of wavefield extrapolation, each using local straight raypaths, simulates propagation along all possible paths.

CONCLUSIONS

Space-frequency domain expressions for the major phase-shift operators have been presented and shown to correspond to local Kirchhoff summation operators. These

operators are easily adapted to accommodate strong velocity heterogeneity, although the extension to anisotropy is anticipated to require more research. Formulae for the Kirchhoff equivalent of the Fourier methods of NSPS, PSPI, and Weyl extrapolation were given in 3-D and 2-D.

Numerical experiments were presented in 2-D to compare the Fourier and Kirchhoff method. The Kirchhoff approach was shown to give very similar results to the Fourier techniques and the importance of including the near-field term was demonstrated. Cost comparisons were shown that suggest that considerable efficiencies can be gained by the Kirchhoff approach. Since the cost of recursive Kirchhoff is essentially independent of the velocity complexity, it is a good candidate algorithm for depth migration in complex media.

RESEARCH PLANS

In the coming year we intend to implement and test a 3D prestack depth migration code using the recursive Kirchhoff approach. This will be done on a parallel system of workstations using a Fortran code.

ACKNOWLEDGEMENTS

Funding for this work came from CREWES, NSERC, and MITACS and we thank all of these organizations. Hugh Geiger provided helpful advice and consultation.

REFERENCES

Berkhout, A.J., 1981, Wave field extrapolation techniques in seismic migration, a tutorial: Geophysics, **46**, 1638-1656.

Berkhout, A.J., 1985, Seismic Migration: Imaging of acoustic energy by wave field extrapolation: in Developments in Solid Earth Geophysics, Vol. 14A, Elsevier.

Bevc, D. 1997, Imaging complex structures with semirecursive Kirchhoff migration: Geophysics, **62**, 577-588.

Biondi, B. and Vaillant, L., 2000, 3-D wave-equation prestack imaging under salt: Expanded Abstracts, 70th Ann. Internat. Mtg: Soc. of Expl. Geophys., 906-909.

Blesitein, N. and Handselman, R.A., 1986, Asymptotic Expansions of Integrals: Dover Press.

Dickens, T.A. and Willen, D.E., 2000, A path-integral approach to depth migration: Expanded Abstracts, 70th Annual SEG Mtg., 846-849.

Docherty, P., 1991, A brief comparison of some Kirchhoff integral formulas for migration and inversion: Geophysics, Soc. of Expl. Geophys., **56,** 1164-1169.

Ferguson, R.J. and Margrave, G.F., 2001, Prestack depth imaging by symmetric nonstationary phase shift: Geophysics, *in press.*

Gazdag, J., 1978, Wave equation migration with the phase-shift method: Geophysics, Soc. of Expl. Geophys., **43,** 1342-1351.

Gradsteyn, I.S., and Ryzhik, I.M., 1980, Table of Integrals, Series, and Products: Academic Press, ISBN 0-12-294760-6.

Gray, S.H., 1997, True-amplitude seismic migration: A comparison of three approaches: Geophysics, Soc. of Expl. Geophys., **62,** 929-936.

Hagedoorn, J.D., 1954, A process of seismic reflection interpretation: Geophys. Pros., **2**, 85-127.

Margrave, G.F. and Ferguson, R.J., 1998, Explicit Fourier wavefield extrapolators: 10th Annual CREWES Research Report.

Margrave, G.F. and Ferguson, R.J., 1999, Wavefield extrapolation by nonstationary phase shift: Geophysics, 64, 1067-1078.

Margrave, G.F. and Ferguson, R.J., 2000, Taylor series derivation of nonstationary wavefield extrapolators: 70th Annual SEG meeting, Calgary, Ab., 834-837.

Morse, P.M. and Feshbach, H., 1953, Methods of Theoretical Physics, McGraw-Hill, ISBN
Murray, J.D., 1984, Asymptotic Analysis, Springer, ISBN 0-387-90937-0.
Robinson, E.A. and Silvia, M.T., 1981, Digital Foundations of Time Series Analysis: Wave Equation Space-Time Processing: Holden-Day, ISBN 0-8162-7271-9.
Schneider, W.A., 1978, Integral formulation for migration in two dimensions or three dimensions: Geophysics, **43**, 49-76.
Stein, E.M., 1993, Harmonic analysis: real-variable methods, orthogonality, and oscillatory integrals: Princeton University Press.
Weyl, H., 1931, The Theory of Groups and Quantum Mechanics: Dover edition (pub 1950).
Wong, M.W., 1998, Weyl Transforms: Springer, ISBN 0-387-98414-3.
Wyatt, K., DeSantis, J., Valasek, P., Chen, C., Shen, Y., Meng, Z., Branham, K., Fromyr, E., and Delome, H., 2000, A 3-D wavefield imaging experiment in the deepwater Gulf of Mexico, Expanded Abstracts, 70th Ann. Internat. Mtg: Soc. of Expl. Geophys., 854-857.
Zauderer, E., 1989, Partial Differential Equations of Applied Mathematics: John Wiley, ISBN 0-471-31516-8.

FIGURES

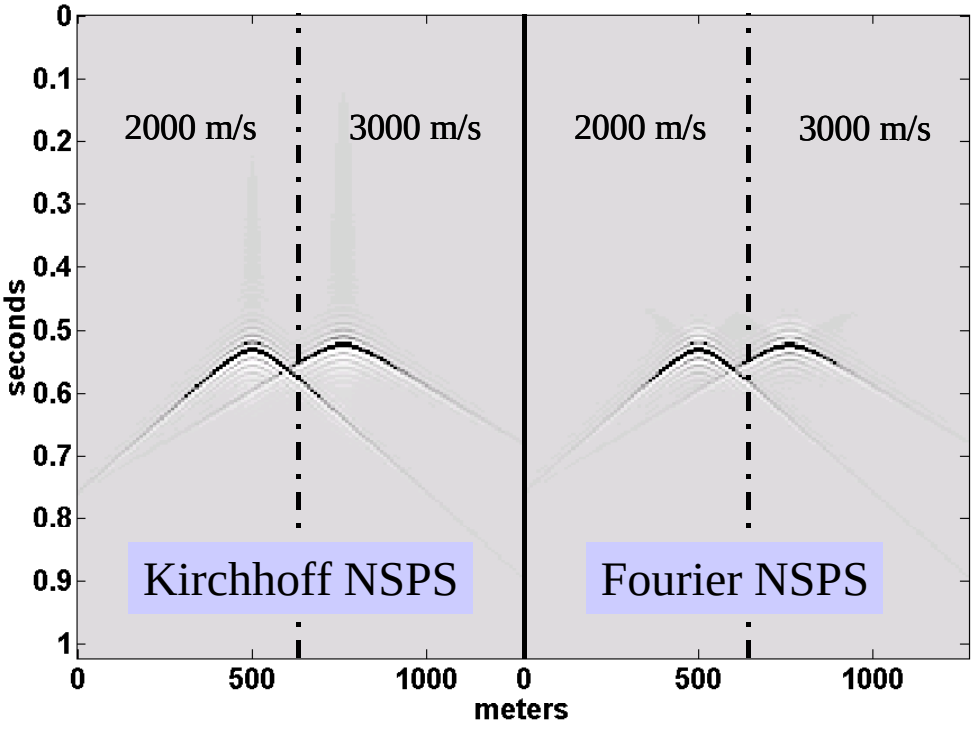

FIG. 1. The Kirchhoff NSPS algorithm is compared with its Fourier counterpart. A single upward step of 50m was taken through a bimodal velocity model. The dashed line separates a 2000m/s medium from a 3000m/s medium. The input wavefield contained two isolated impulses, one in each medium.

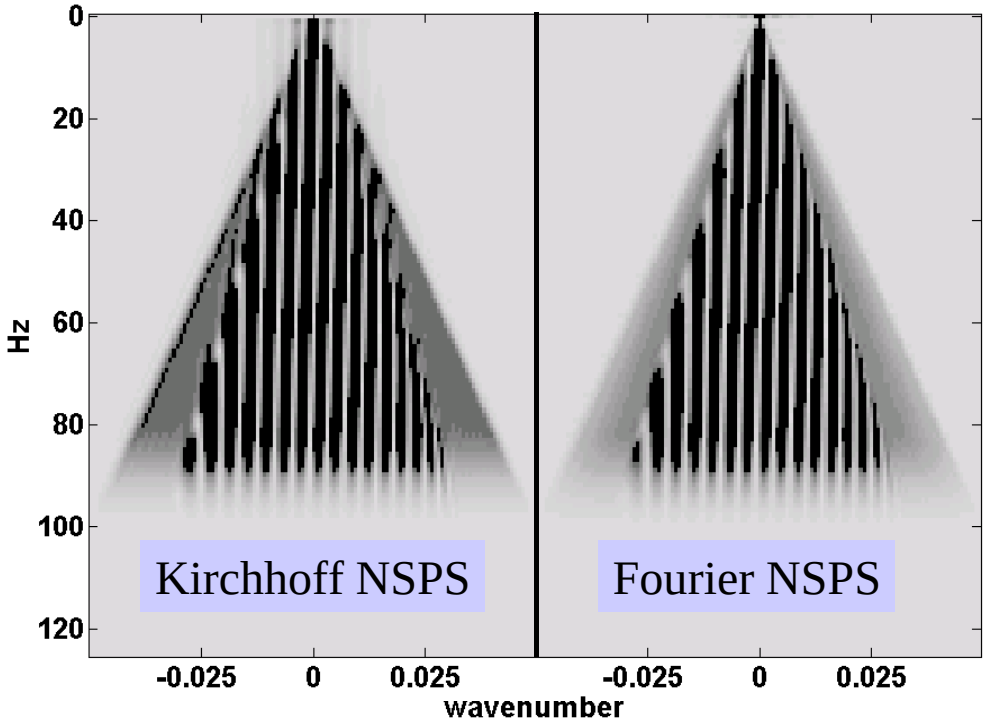

FIG. 2. The *f-k* amplitude spectra of the wavefields of Figure 1.

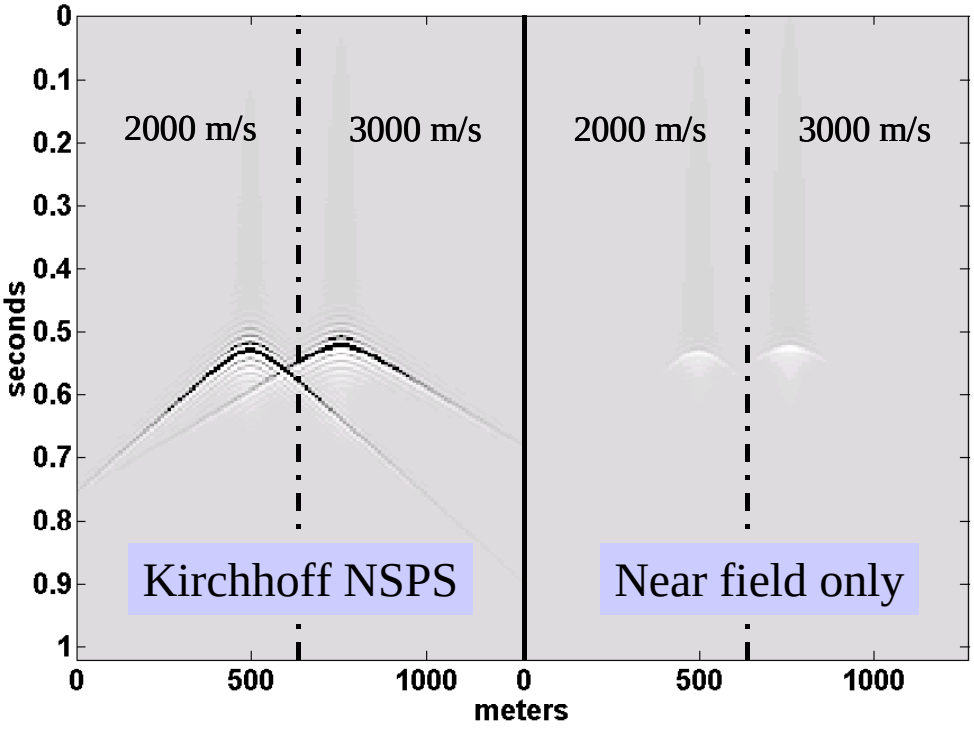

FIG. 3. On the left is a repeat of the left side of Figure 1 while the right side contains the near-field term only. The near-field is quite small compared with the total field.

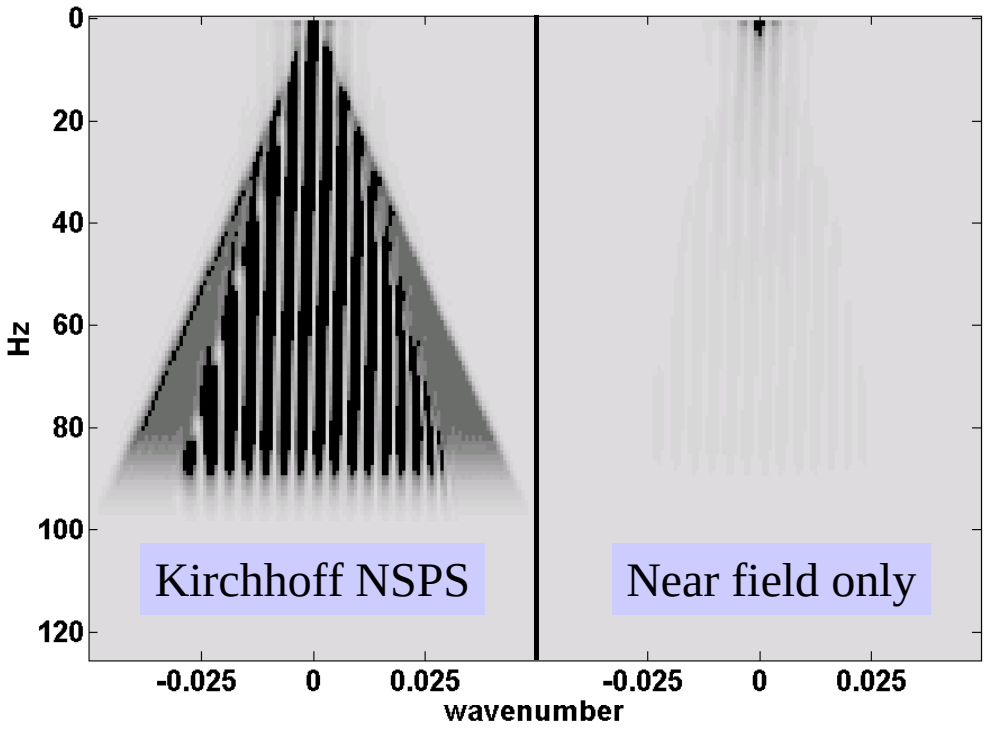

FIG. 4. The *f-k* amplitude spectra of the wavefields of Figure 3.

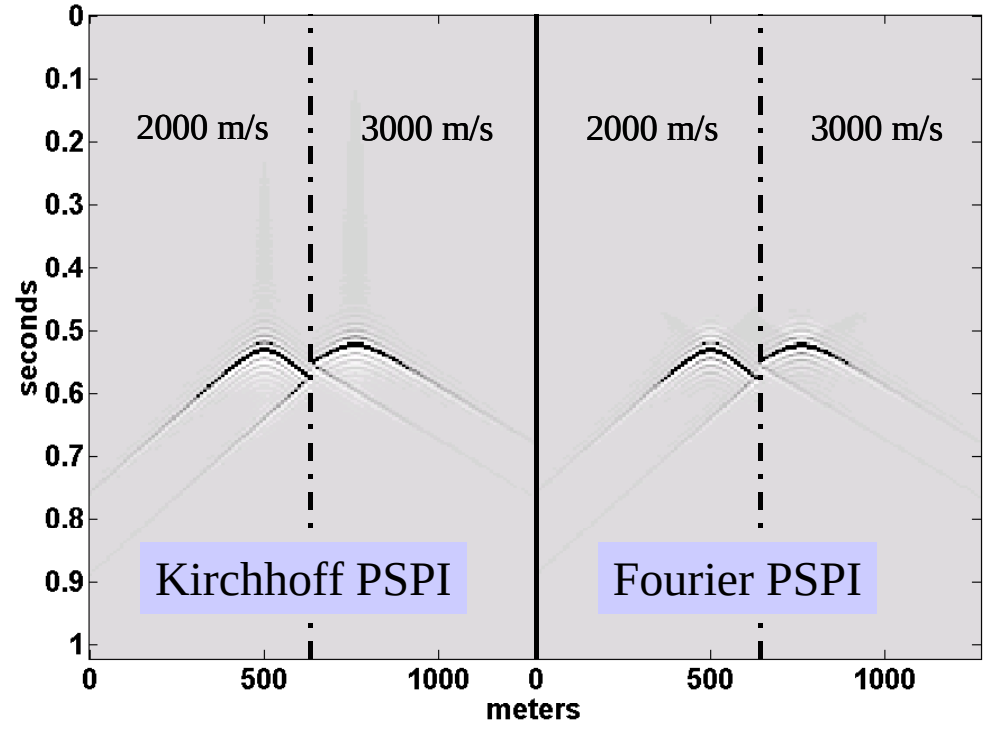

FIG. 5. This is a repeat of the example of Figure 1 except that the PSPI algorithm has been used.

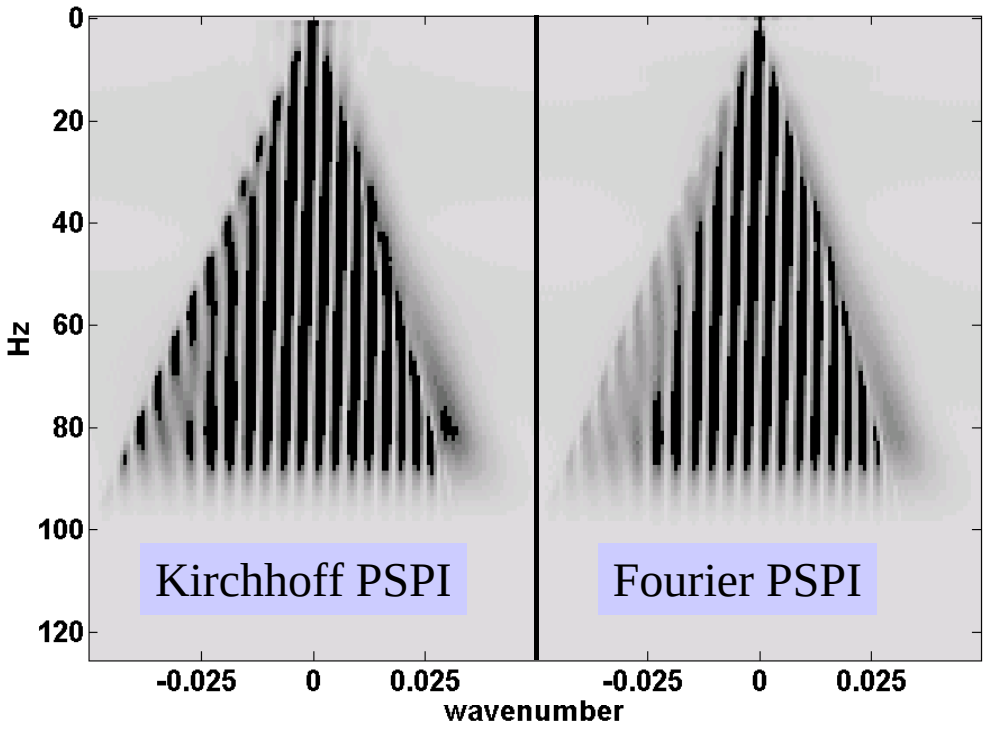

FIG. 6. The *f-k* amplitude spectra of the wavefield of Figure 5 are shown.

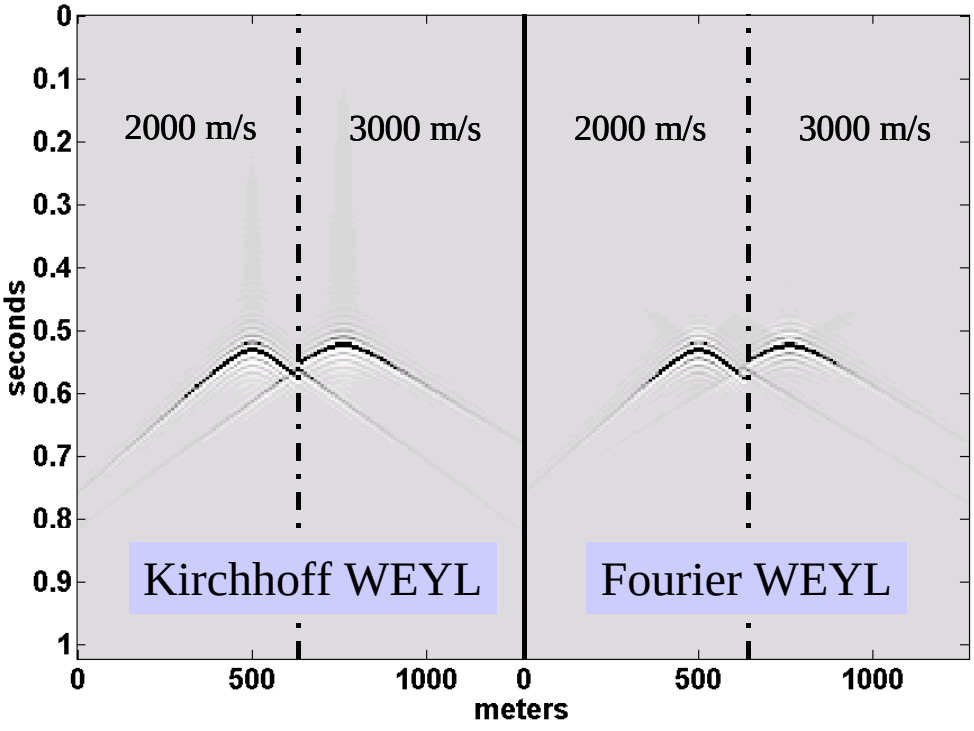

FIG. 7. The experiment of Figures 1 and 5 has been repeated using the Weyl operator. This averages the behaviour of the previous two operators.

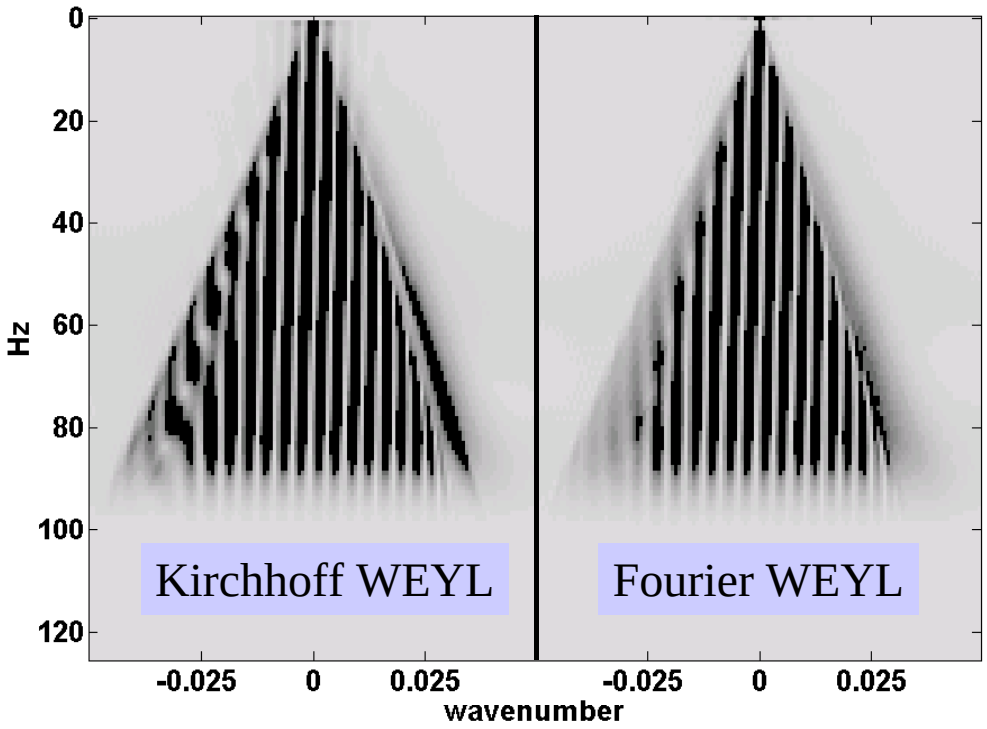

FIG. 8. The *f-k* amplitude spectra of the wavefields of Figure 7 are shown.

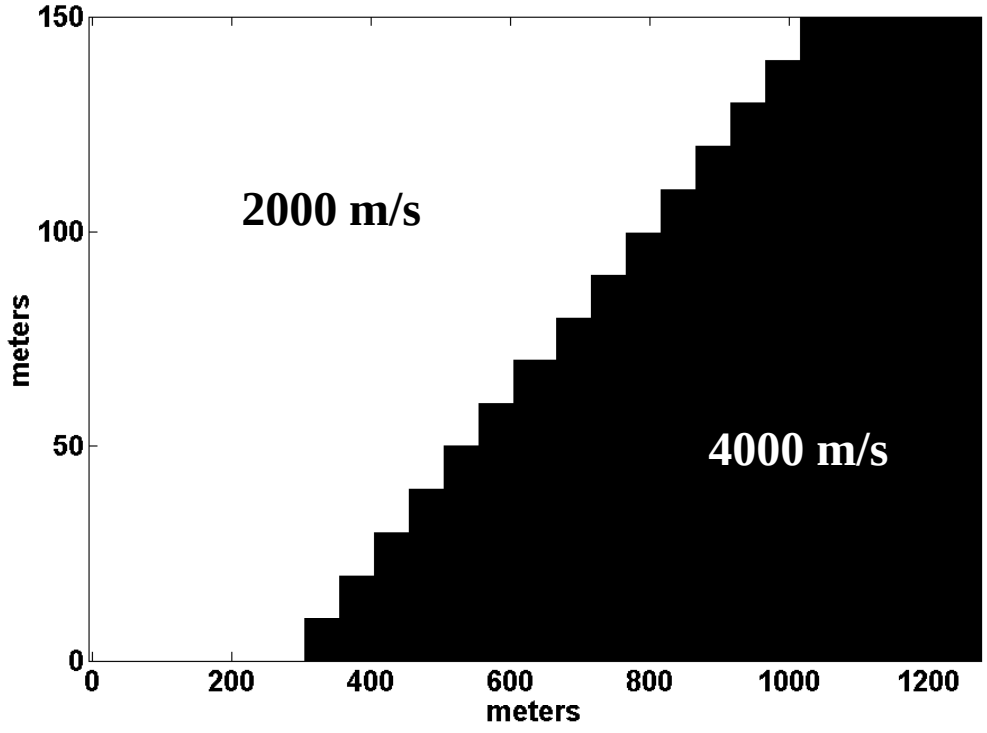

FIG. 9. A “fault” velocity model.

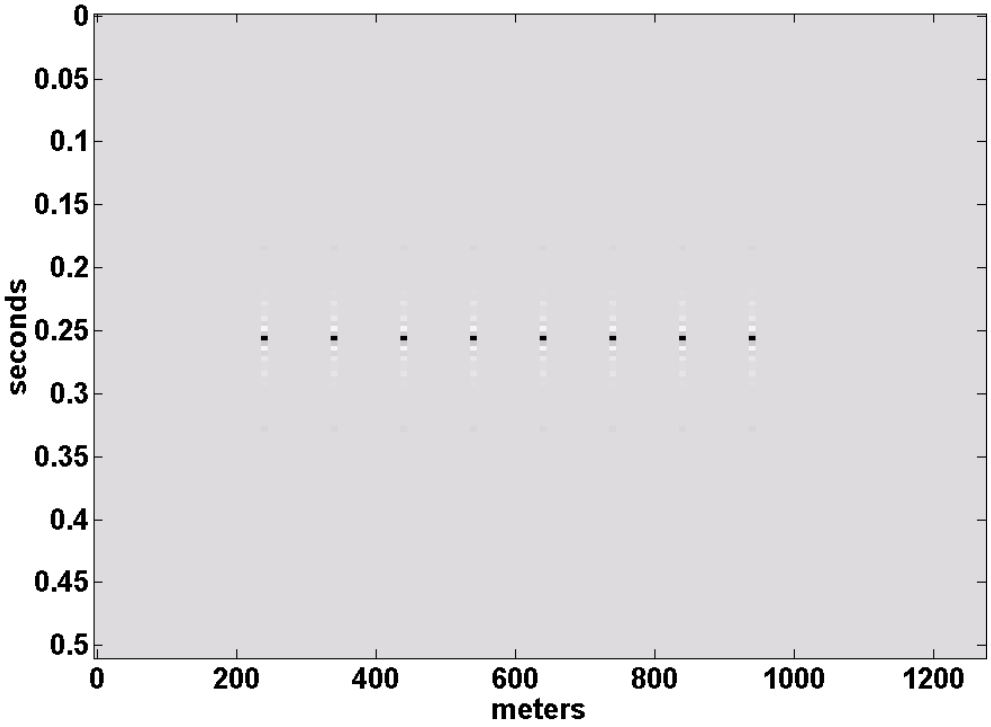

FIG. 10. The input wavefield to a series of wavefield extrapolation experiments.

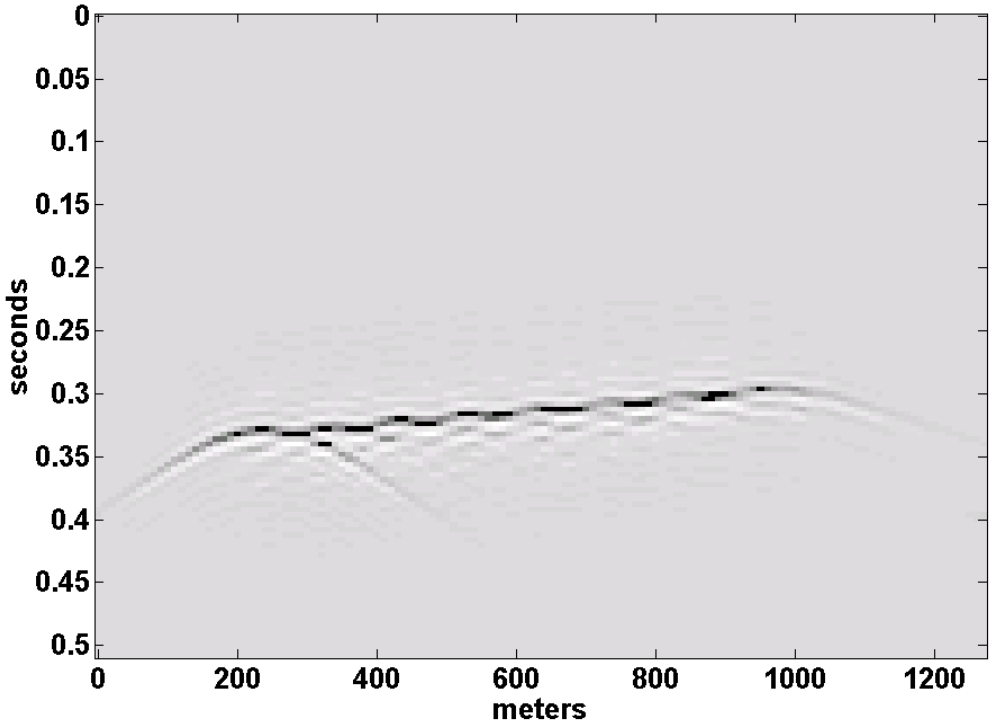

FIG. 11. The result of the upward extrapolation of the wavefield of Figure 10 through the velocity model of Figure 9. Fifteen upward steps of ten metres each were taken with the Fourier NSPS algorithm.

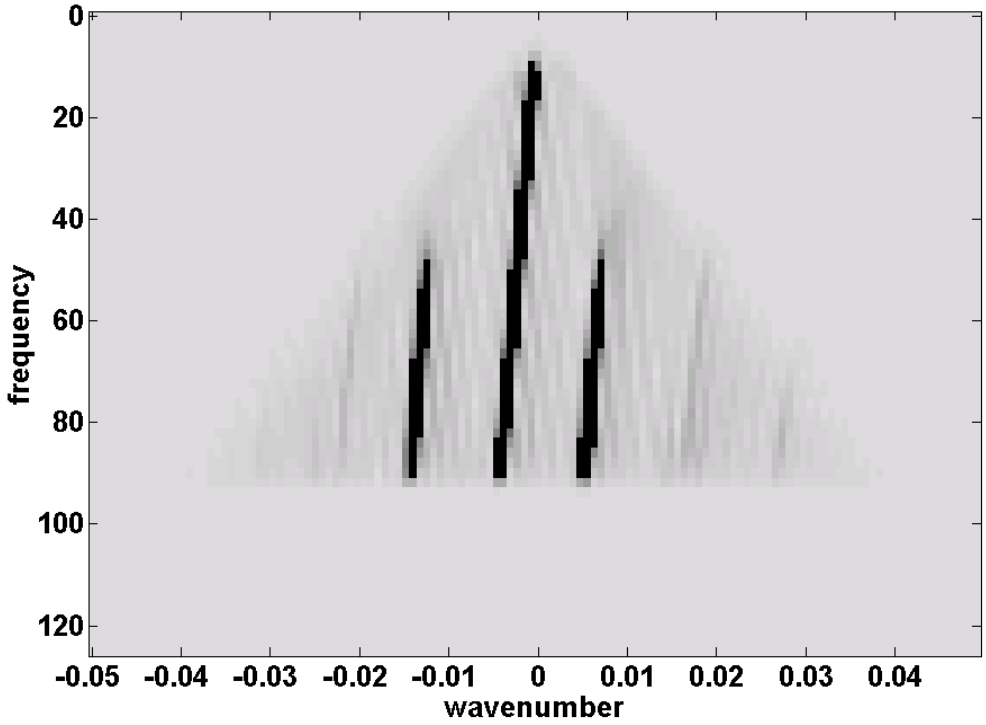

FIG. 12. The *f-k* magnitude spectrum of the wavefield of Figure 11. Note the tilt of the spectral lines to the left.

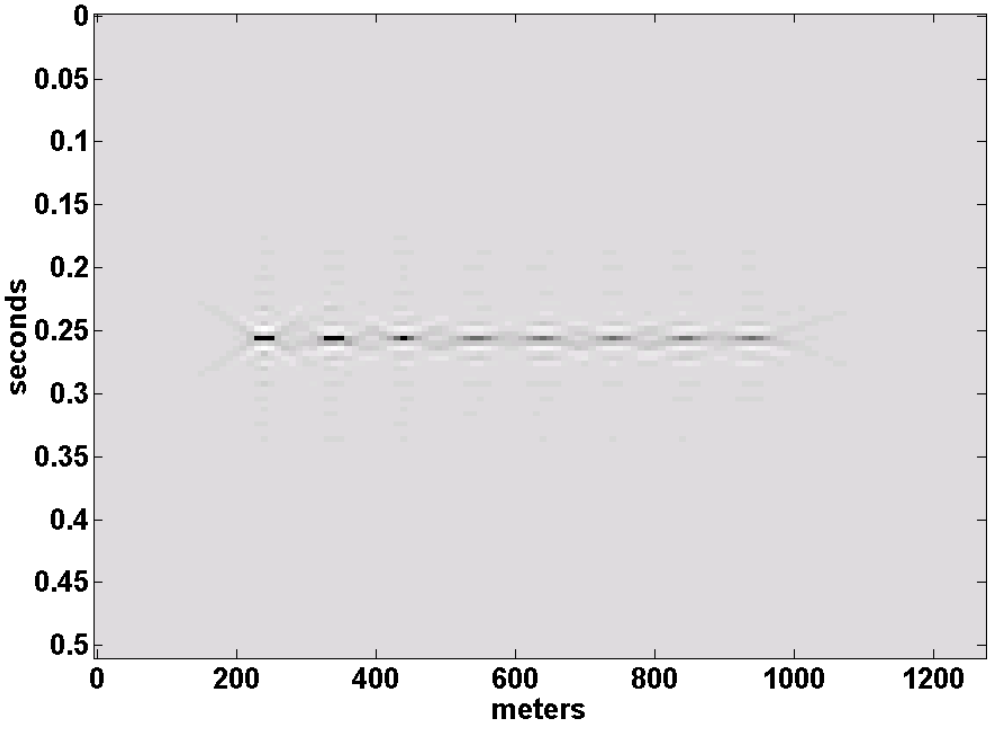

FIG. 13. The result of a downward extrapolation of the wavefield of Figure 11 with the Fourier PSPI algorithm using 5-30m steps.

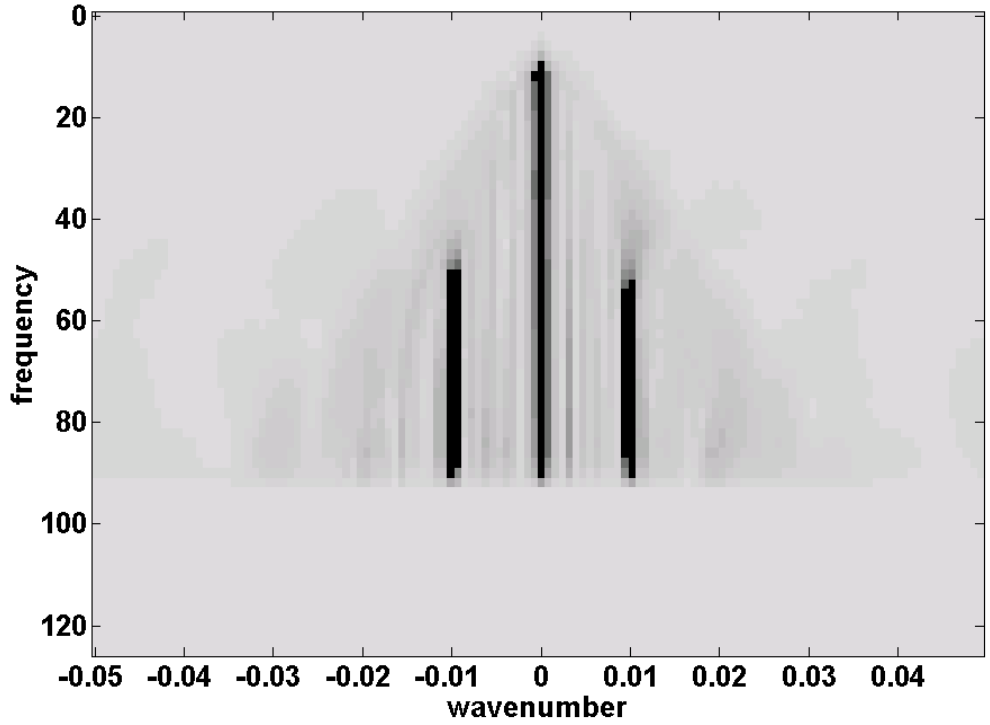

FIG. 14. The *f-k magnitude* spectrum of the wavefield of Figure 13.

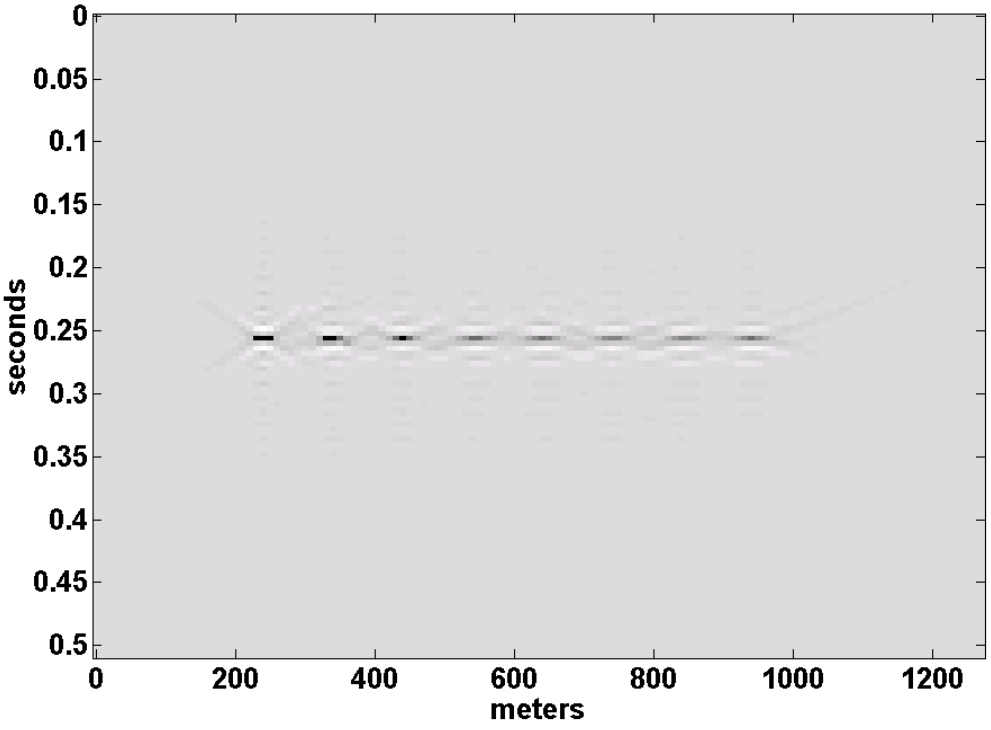

FIG. 15. A downward extrapolation with Kirchhoff PSPI, including the near-field term, using 5-30m steps of the wavefield of Figure 11.

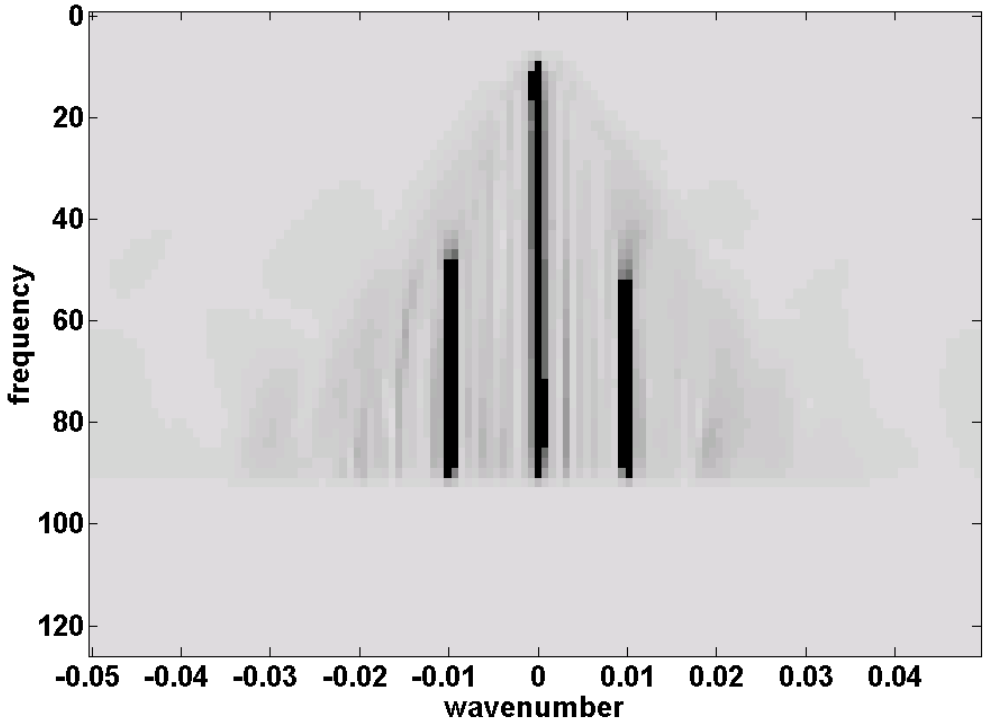

FIG. 16. The *f-k* magnitude spectrum of the wavefield of Figure 15.

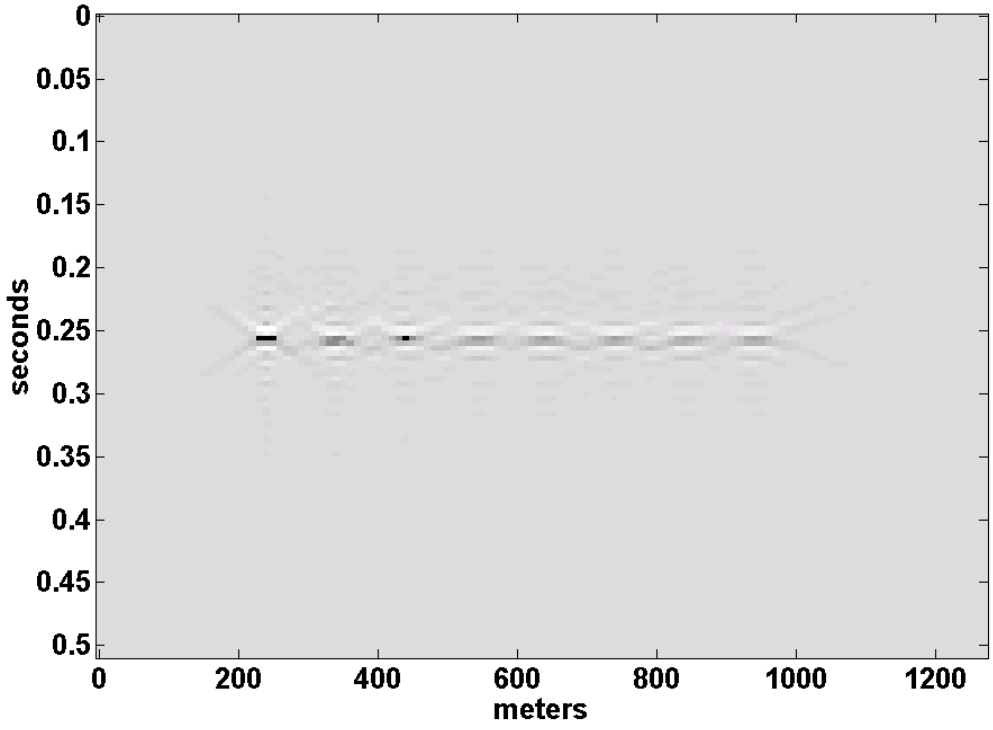

FIG. 17. A Kirchhoff NSPS extrapolation of the wavefield of Figure 11, identical in all respects to the extrapolation of Figure 15 except that the near-field term was omitted.

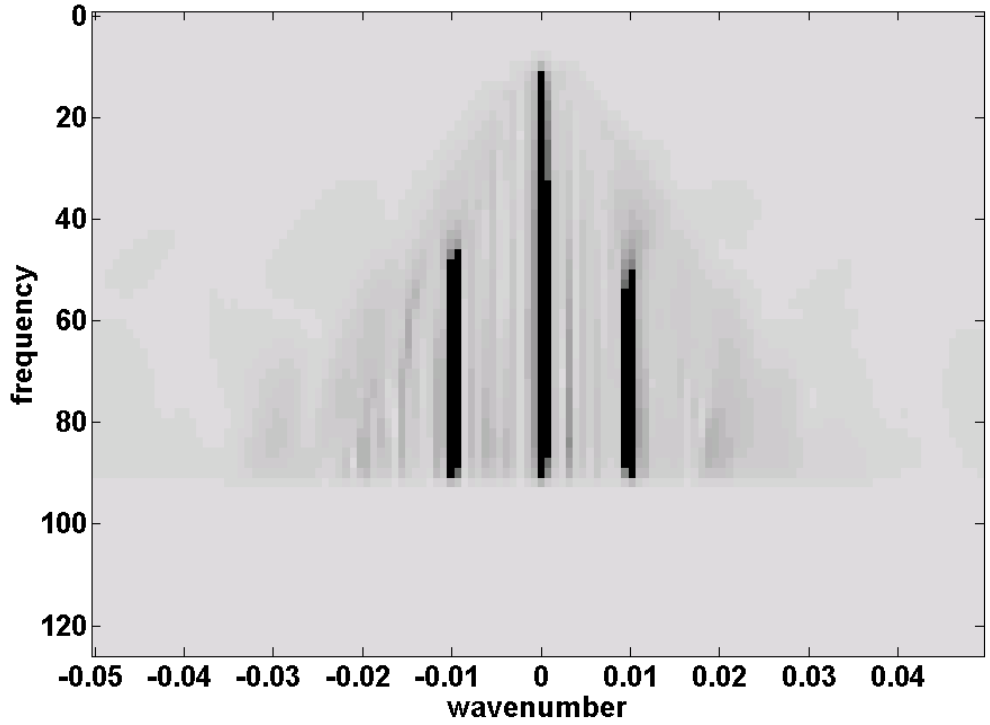

FIG. 18. The *f-k* spectrum of the wavefield of Figure 17.

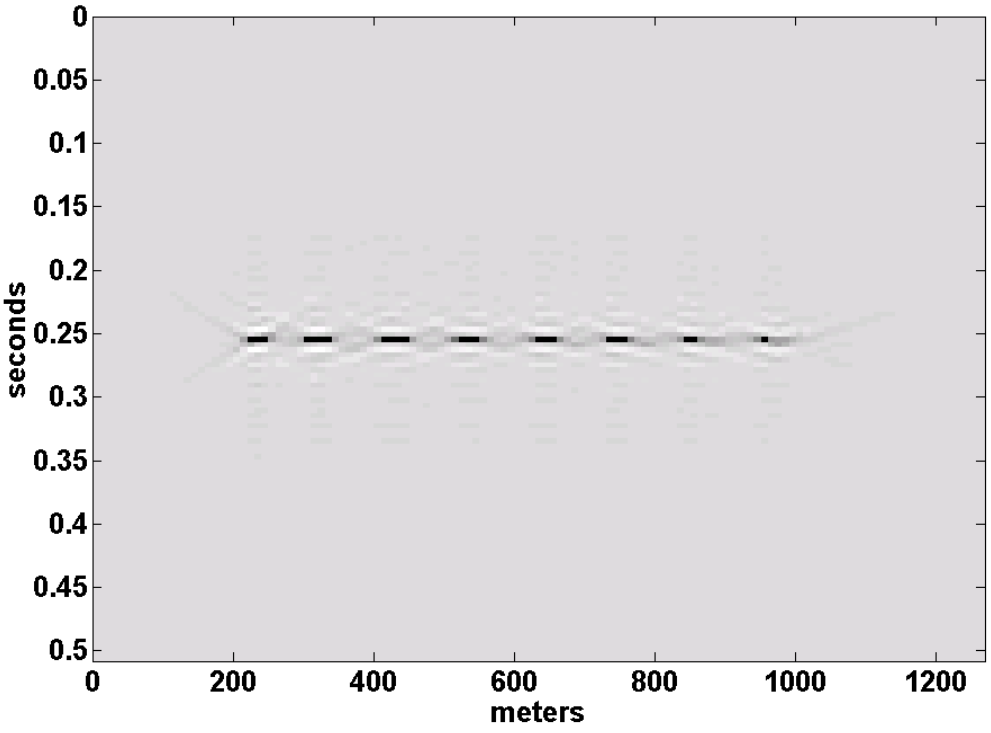

FIG. 19. The downward extrapolation, using Fourier PSPI and 15-10m depth steps, of the wavefield of Figure 11.

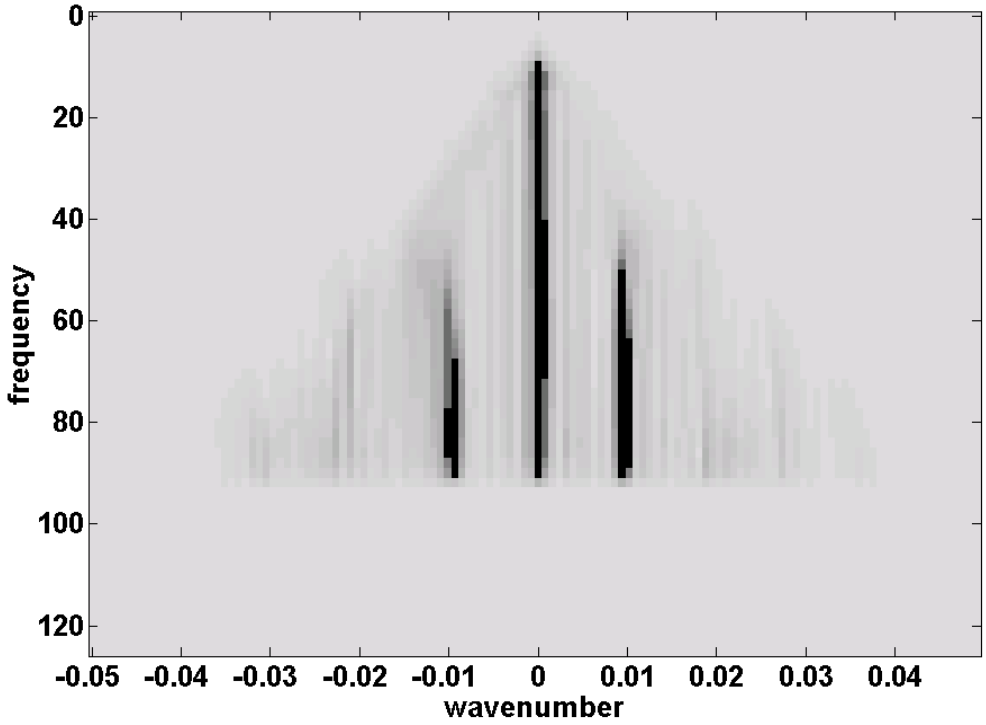

FIG. 20. The *f-k* spectrum of the wavefield of Figure 19.

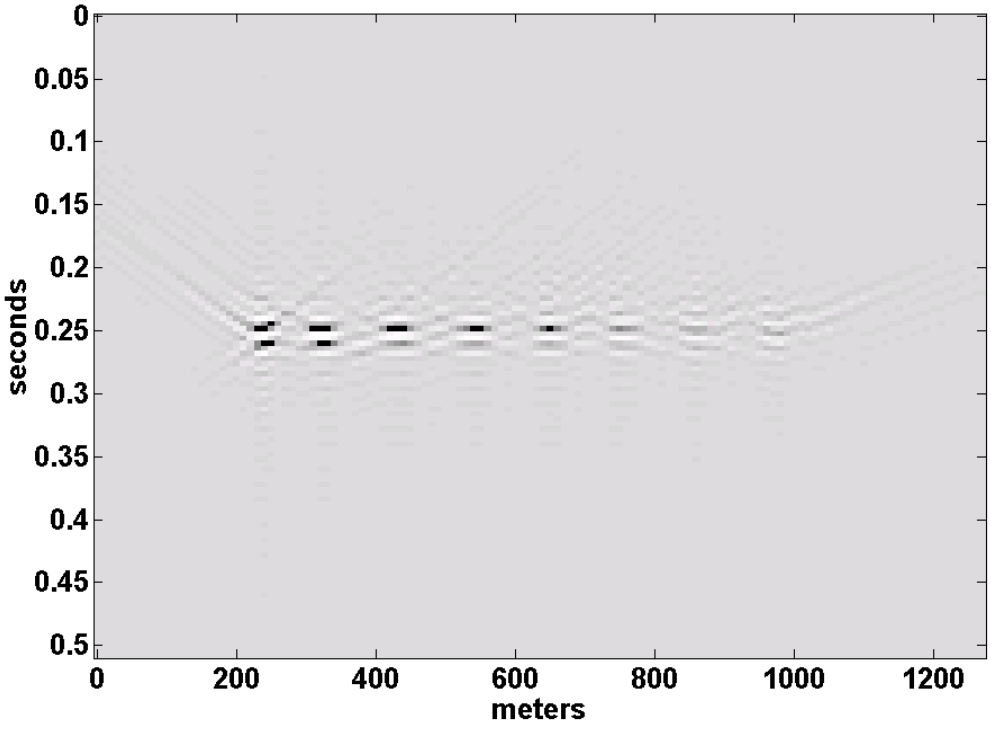

FIG. 21. The result of 15-10m steps with Kirchhoff PSPI, without the near-field term, of the wavefield of Figure 11.

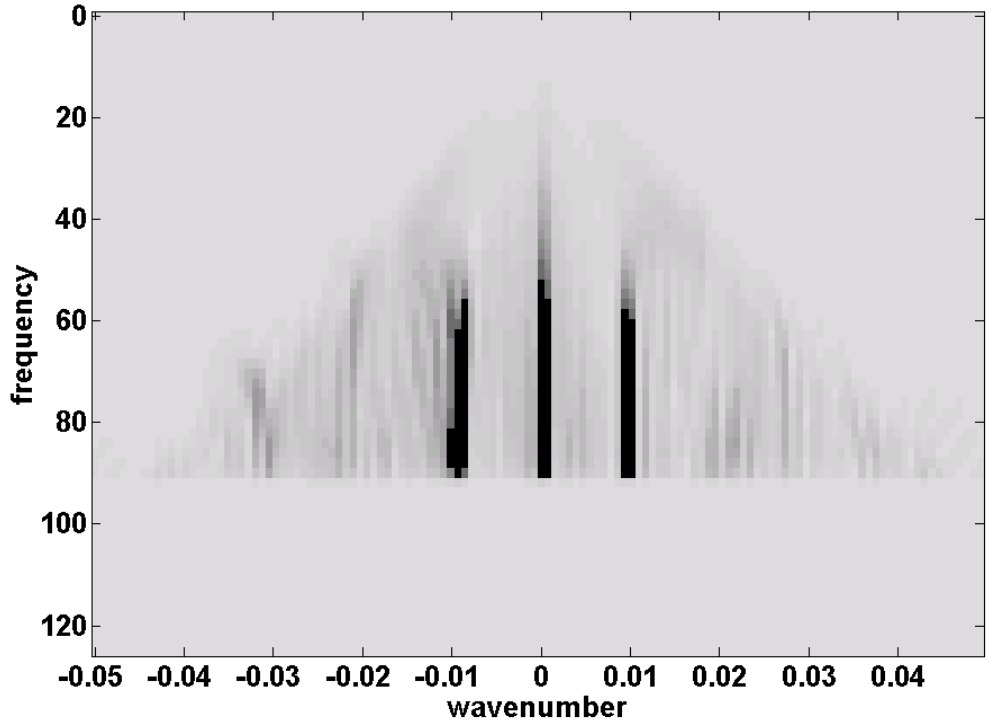

FIG. 22. The *f-k* spectrum of the wavefield of Figure 21.

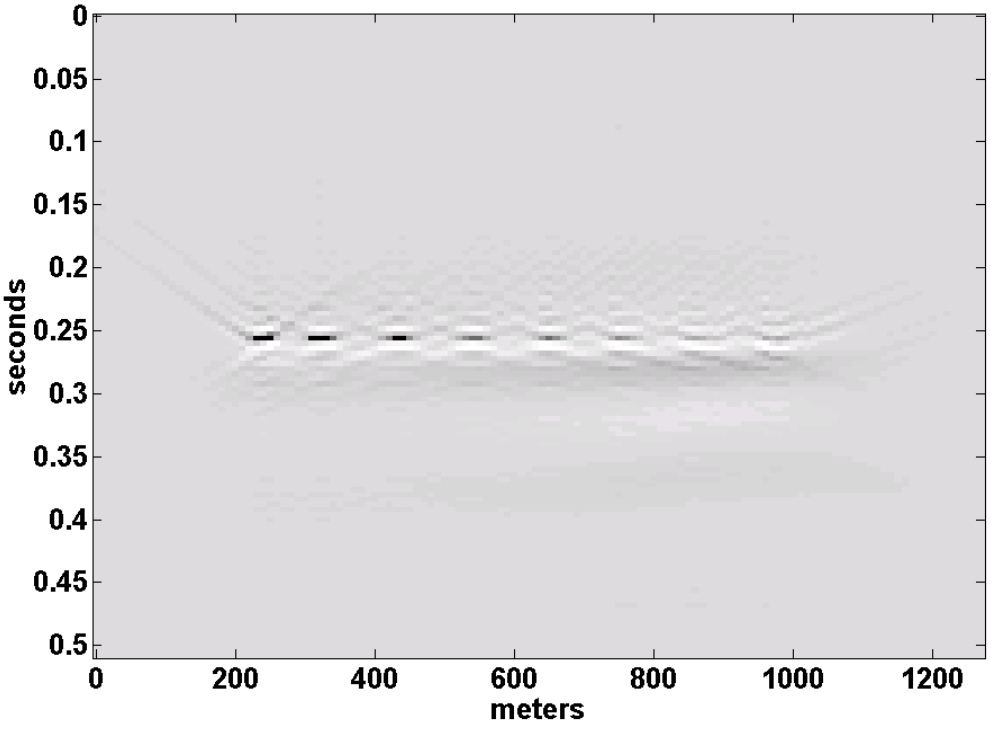

FIG 23. The result of 15-10m steps of Kirchoff NSPS, including the near-field term, of the wavefield of Figure 11.

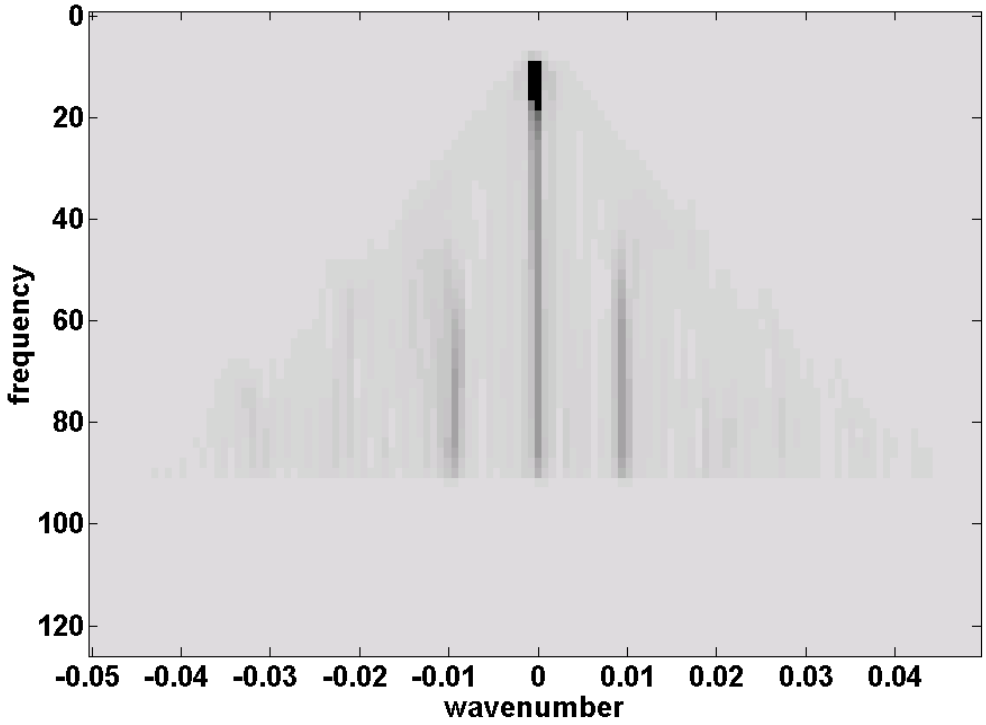

FIG. 24. The *f-k* spectrum of the wavefield of Figure 23.

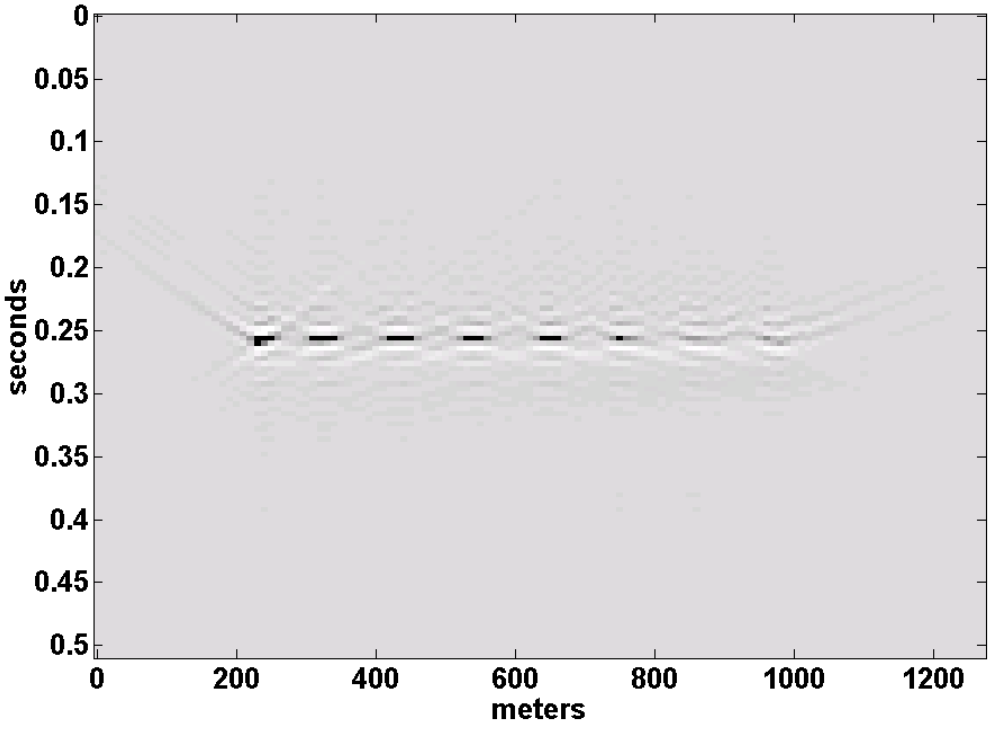

FIG. 25. A repeat of the experiment of Figure 21 except that only 80% of the near-field term was included.

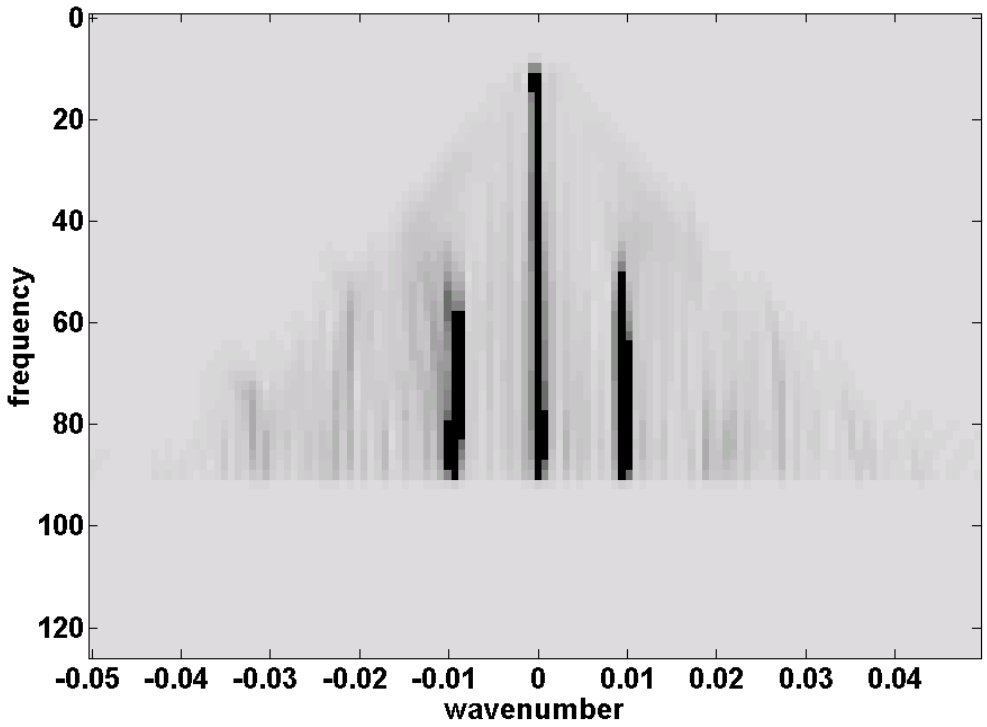

FIG. 26. The *f-k* spectrum of the wavefield of Figure 25.

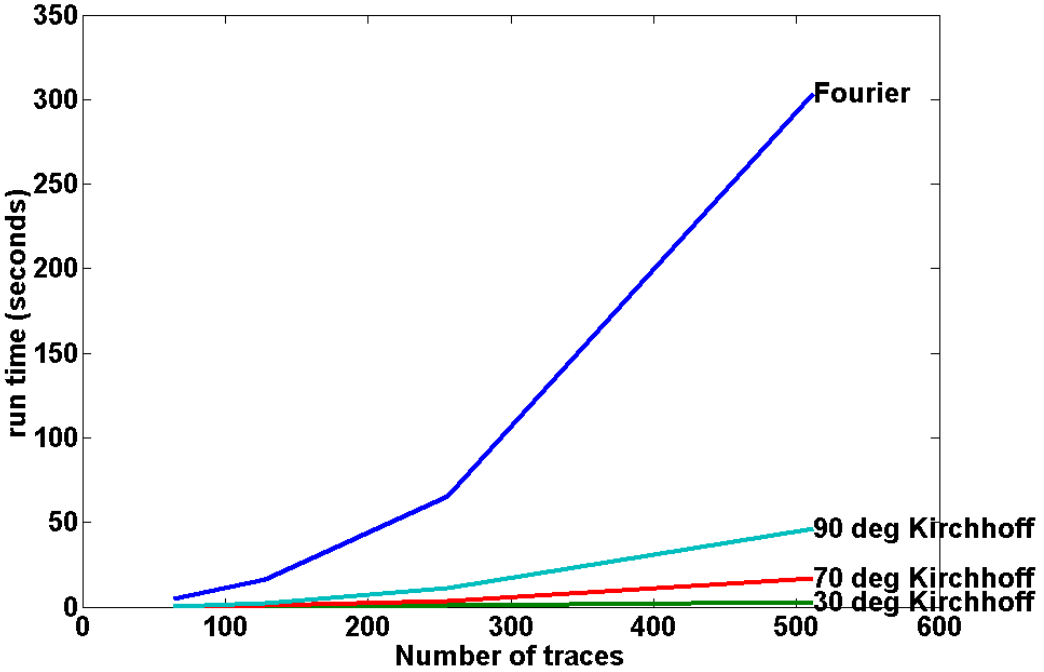

FIG. 27. The result of run-time testing for the Fourier NSPS algorithm and its Kirchhoff equivalent using three different dip limits. Four experiments were run using 64,128, 256, and 512 traces each.

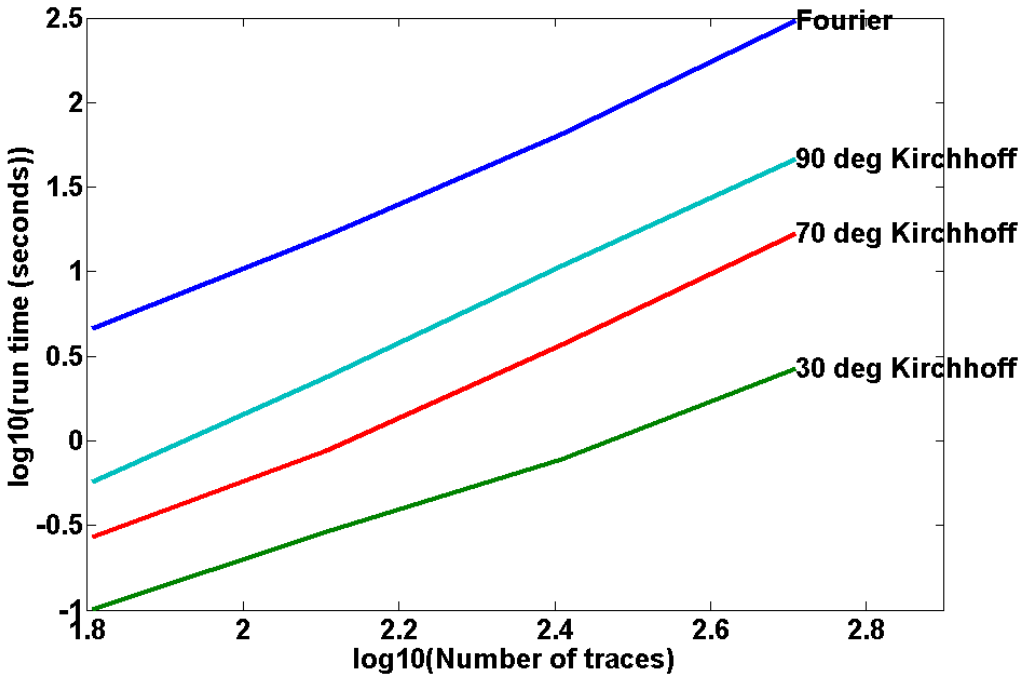

FIG. 28. The data of Figure 27 have been plotted with logarithmic scales on both axes. All methods have a slope of about 2 indicating that they scale as the square of the number of traces.

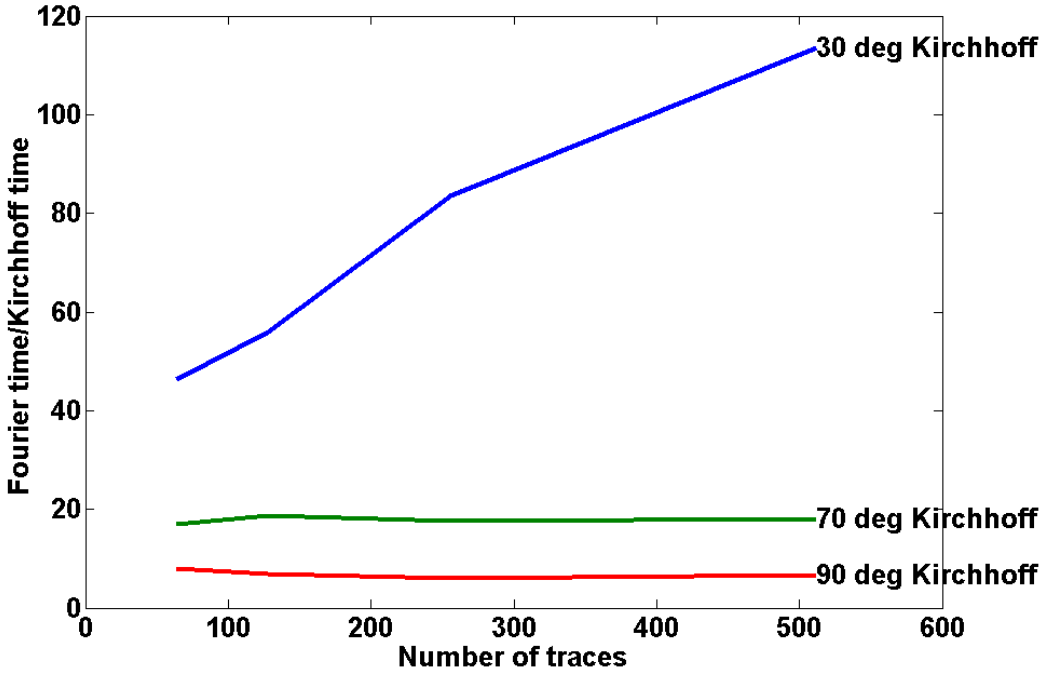

FIG. 29. The data of Figure 27 are displayed as the ratio of the Fourier time to the Kirchhoff time. The 30-degree algorithm is as much as 100 times faster while the 90-degree algorithm is about 6 times faster.